Specific Heat of Dilute Alloys of the Transition Metals in Nickel*

René Caudron, Renaud Caplain, Jean-Jacques Meunier, and Paul Costa
Office National d'Etudes et de Recherches Aérospatiales, 92320 Châtillon, France
(Received 9 March 1973)

The specific heat of nickel-based dilute alloys with the metals of the three transition series have been measured in the 1.2–10-K range with a precision of 0.1%. The electronic-specific-heat coefficient increases per unit impurity concentration at infinite dilution (in mJ/K^2 mole per unit atomic concentration) are $d\gamma/dc|_0 = 18, 30, 43, -13$ for Ti, V, Cr, Mn, respectively (first series). For the second series, we found 35, 48, 40, − 1.5, 2.5 for Nb, Mo, Ru, Rh, and Pd. For the third series (Ta, W, Re, Os, Ir, and Pt) the results are 34, 44, 54, 69, 29, and 14. In the three series, a strong γ increase is to be noticed when the virtual bound state repelled by the impurity potential from the majority-spin band $d\uparrow$ crosses the Fermi level. However, the agreement with the present state of the theory is only qualitative; it was found that when the virtual bound state sits at the Fermi level, the $d\gamma/dc|_0$ values are much higher than expected. They remain important when the virtual bound state is well above the Fermi level, the expected value being zero in this case. The same qualitative agreement and quantitative discrepancies between theory and experiment also arise for nonmagnetic impurities in non-transition-metal matrices.

I. INTRODUCTION

The description of transition-metal impurities dissolved in strong ferromagnets such as nickel and cobalt has already been given, at least qualitatively, by several authors[1]: The impurity d states, hybridized with states of the matrix of the same symmetry, behave differently, depending on the strength of the repulsive potential localized on the impurity cell, which is mainly a function of the valency difference between the impurity and the matrix. If the potential is not too strong, the impurity states merge into the band states of the matrix. If, on the contrary, the potential is strong enough, bound levels are extracted from the band. Their hybridization with the matrix states leads to a spatial extension, which is larger if the bound state lies closer to the limits of the band. The energy of these states is however perfectly defined if we restrict ourselves to a non-interacting d-d model. The energy broadening comes from s-d mixing (the states are then said virtual bound states).[2] This broadening is of about 0.5 eV, so that the two bound levels corresponding to Γ'_{25} and Γ_{12} symmetries merge into a single virtual level with room for five electrons.

Both situations can simultaneously occur in a strong ferromagnetic matrix, since the Fermi states then belong to one spin direction only ($\downarrow$). For the opposite direction ($\uparrow$), the d states are fully occupied, and lead to a band which is shifted with respect to the ($\downarrow$) band as a result of the exchange interaction between electrons. While the ($\downarrow$) impurity d states can only merge into the ($\downarrow$) continuum of the matrix, one may expect the ($\uparrow$) impurity states either to interact in the same way with the ($\uparrow$) band, or to yield bound states which lie higher than the top of the band.

We can draw with reasonable confidence information about the actual situation for each type of impurity from saturation magnetic moment measurements: If Z is the excess positive charge located on the core of the impurity, it is related to the $Z_\uparrow$ and $Z_\downarrow$ values of the displaced charge in the ($\uparrow$) and ($\downarrow$) bands by

$$Z = Z_\uparrow + Z_\downarrow \quad \text{(Friedel's rule)} .$$

Since the variation of the magnetic moment per unit impurity $\Delta\mu$ is also related to $Z_\uparrow$ and $Z_\downarrow$ by a linear relation

$$\Delta\mu = \mu_B(Z_\uparrow - Z_\downarrow) ,$$

one can deduce the $Z_\uparrow$ and $Z_\downarrow$ values.

For the metals of the first transition series dissolved in nickel, these measurements yield the following results: $Z_\uparrow = 0$ for cobalt, iron and manganese -4 for chromium, -5 for titanium and vanadium. We can then conclude that for the last two metals a fivefold degenerate d virtual bound level has been extracted and is sitting above the Fermi level. For chromium, it is only partly filled with approximately one state out of five being occupied.

In the second series, similar phenomena take place, but occur for smaller values of $|Z|$. This "period effect," already described by Demangeat and Gautier,[3] is due both to the larger spatial extension of the impurity d states and to the higher value of the corresponding energy of the free atom. For ruthenium ($Z = -2$), Crangle[4] has found $Z_\uparrow = -2.5$, which clearly proves that the ($\uparrow$) impurity state sits as a half-filled virtual bound level at the Fermi level. For osmium (third series, $Z = -2$), $Z_\uparrow = -2$, indicating again the emptying of the vir-

tual bound state.

Extra information can also be drawn from transport properties through an analysis of the deviations from Matthiessen's law. As in any transition metal, the s electrons are the main current carriers, but relaxation processes for $s_\uparrow$ and $s_\downarrow$ subbands are different. If $s_\uparrow$ and $s_\downarrow$ currents are taken as parallel and independent, and if Matthiessen's law is obeyed in each subband, one should not expect it to be obeyed on the whole for the total current (in this case, conductances are additive, not resistances). Besides, intraband relaxation processes between $s_\uparrow$ and $s_\downarrow$, primarily due to electron-magnon interaction, lead to a mixing of the two currents with a total resistivity

$$\rho = \frac{\rho_\uparrow\rho_\downarrow + \rho_{\uparrow\downarrow}(\rho_\uparrow + \rho_\downarrow)}{\rho_\uparrow + \rho_\downarrow + 4\rho_{\uparrow\downarrow}}$$

(notice that diffusion of s electrons with spin-flip by magnons is the main contribution to $\rho_{\uparrow\downarrow}$, but is also present in $\rho_\uparrow$ and $\rho_\downarrow$).

For dilute alloys with noninteracting impurities, one can write

$$\rho_\alpha = \rho_{m\alpha} + c\rho_{0\alpha}, \quad \rho_{\uparrow\downarrow} \simeq \rho_{m\uparrow\downarrow},$$

where α stands for the spin direction, $\rho_{m\alpha}$ is the corresponding resistivity term of the matrix, c is the impurity concentration, and $\rho_{0\alpha}$ is the α resistivity induced by the impurity per unit concentration. It is then possible to reach separately the values for $\rho_{0\uparrow}$ and $\rho_{0\downarrow}$, either through the dependence of ρ upon concentration at a given temperature, or by performing experiments at a temperature for which $c\rho_0 \gg \rho_m$, $\rho_{\uparrow\downarrow}$ ($T \simeq 4$ K), and then at a temperature for which $\rho_m, \rho_{\uparrow\downarrow} \gg c\rho_0$ (low concentration, room temperature), or by working on alloys including two types of impurities.

A similar analysis of the thermoelectric power S has been derived by Cadeville and Roussel,[5] which leads to the separation of $S_{0\uparrow}$ and $S_{0\downarrow}$, with

$$S_{0\alpha} = \frac{\pi^2 k_B^2 T}{3|e|}\left(\frac{\partial \ln\rho_{0\alpha}}{\partial E}\right)_{E=E_F}.$$

In the case of nickel-based alloys, the experiments performed by Fert and Campbell,[6] and Durand and Gautier,[7] show that a maximum value of $\rho_{0\uparrow}$ occurs when the virtual bound state crosses the Fermi level (as indicated by magnetic moment measurements): chromium in the first series, ruthenium in the second, osmium in the third. The thermoelectric power results are in agreement with the latter description: $S_{0\uparrow}$ is negative when $|Z_\uparrow| < 2.5$ (the virtual bound state is more than half-filled), and positive when $|Z_\uparrow| > 2.5$: $S_{0\uparrow} = +50$ μV/K for chromium ($Z_\uparrow = -4$) and -17 for osmium ($Z_\uparrow = -2$).

More experimental evidence of the above described electronic structure can be obtained from electronic-specific-heat experiments. When the virtual bound state crosses the Fermi level, we can expect an increase in the density of states, this being proportional to the impurity concentration in the $c = 0$ limit, and showing a nonlinear behavior due to pair or cluster effects at higher concentrations. The purpose of this work is to find these modifications of the density of states at the Fermi level through low temperature measurements of the electronic-specific-heat coefficient γ.

II. SAMPLES

A. Choice of Alloys

We have investigated dilute nickel base alloys, the solute atoms being elements of one of the three transition series. Seven elements only were discarded: scandium, yttrium, zirconium, and hafnium, which show a very limited solubility in nickel,[8] technetium for the usual obvious reasons, and cobalt and iron which do not show the virtual-bound-state type of behavior in nickel and have already been partly studied.[9,10] More extensive experiments on these alloys will shortly be published.[11]

Low enough concentrations were taken to retain a one phase structure as well as a linear dependence of specific heat on concentration. On the other hand, the effects had to be accurately measured by our specific-heat-equipment, which led us to choose concentrations between 1 and 4 at.%, with a possible reduction if saturation effects showed up.

B. Sample Preparation

The base metal we used was Mond nickel (99.97%), the main impurities being, in wt ppm: carbon 110; iron, 110; copper, 13; sulphur, 15. Because of their low concentration the impurities of the solute metals were of little importance. Owing to different metallurgical properties, vapor pressure for instance in the case of manganese, and the availability of the necessary equipment, the various samples were fused using one of the three following methods; electron-beam melting under 10^{-6}-torr vacuum, arc melting under 300-torr argon pressure, or induction casting under argon pressure. The ingots were then annealed at 1250 °C, under a 1 atm pressure of argon, for 1 to 7 days.

C. Sample Control

All the samples were submitted to metallographic examination, in order to check that no precipitation effects had occurred. Concentrations were checked by several methods: classical chemistry

for titanium, vanadium, chromium, manganese, niobium, molybdenum, tungsten, and tantalum, and x-ray fluorescence for ruthenium, palladium, rhodium, iridium, platinum, and osmium. A further check was made by spectrometric methods for all the alloys of the first and second series. But the correlation between classical chemistry and spectrometric analysis is poor. Besides, the correlation between any of these two types of analysis is poorer than the correlation between γ and the values of the nominal concentration as shown by Figs. (2a) and (2b), which shows that these values give the best estimates of the actual concentration.

III. CALORIMETER

A. Description

Our instrument is a sophisticated version of the classical adiabatic calorimeter we described in a former publication.[12] Three major modifications have been introduced: (a) The sample is inside a sealed vacuum vessel, which allows for a very high, impurity-free vacuum (5×10^{-7} torr when measured at room temperature), obtained by cryopumping. The effect of microleaks is minimized by an auxilliary vacuum jacket surrounding the main vessel. (b) We measured the resistance of the germanium thermometer with a three-wire alternating-current Wheatstone bridge; the detection was made through a lock-in amplifier. This arrangement gives a high temperature sensitivity (better than 3×10^{-5} K) together with a low dissipation on the thermometer, thus avoiding systematic errors in the temperature measurements. (c) The size of the samples was large, which reduced the effect of spurious heat flows (vibrations, rf dissipation, imperfections in the dynamic response of the servo-system which ensures a constant temperature gradient between the sample and its surroundings).

B. Reproducibility

Experiments performed on the same nickel sample after time intervals of several months give results which concur to within 0.1% [see Fig. (1), related to Sec. III D]. But the specific heat of nickel is high and the sample was chosen to be as big as possible: Its heat capacity at 50 K^2 was 160 mJ/K. For a copper sample of about the same weight (heat capacity about three times lower at 50 K^2), the results varied by 0.3%. The nonreproducibilities of our apparatus seem better expressed in terms of heat-capacity fluctuations superimposed on the main measurement.

C. Calibration

The calibration of a thermometer for a specific-heat experiment is always difficult to perform with the required accuracy, since an error of 2 mK on the absolute value of the temperature of the calibration points and an error of 2 mK on the difference in temperature between two points separated by about 1 K would for instance lead to an error of about 0.3% on C_V/T at 2 K. This would give to the specific-heat curve a rather wavy shape, with vague maxima and minima occurring always at the same temperatures. It is then always necessary to remove these systematic errors, which might be taken as a random scatter and overshadow phenomena of minor amplitude, by fitting the results of a series of experiments on a well-known sample to its specific-heat data. In fact, since we had no facilities to calibrate properly the thermometer, we decided to start with its commercial calibration, which gave systematic errors of about 1%, and to improve it by using the results of a series of specific-heat experiments.

Let $f(\Theta) = T - \Theta$ be the difference between the true temperature (T) and the measured temperature (Θ). One can show[13] that, if on performing a heat-capacity measurement the temperature increment $\Delta\Theta$ and the error function $f(\Theta)$ are not too large, the measured specific heat can be expressed by the term $C_m(\Theta) = C_t(\Theta)[1+\varphi(\Theta)]$ where C_t is the true specific heat, and the relative error $\varphi(\Theta)$ is given by

$$\varphi(\Theta) = \frac{df}{d\Theta} + \frac{f}{C_t}\frac{dC_t}{d\Theta} . \tag{1}$$

For materials of similar specific heat laws, $(1/C_t)\,(dC_t/d\Theta)$ does not differ too much from one sample to another. Thus to the same approximation, the φ function for an unknown sample can be reached by performing an experiment on a sample of known heat capacity. Such a process would also include systematic errors of another nature.

This type of calibration is adequate for the comparison of dilute alloys, where the matrix, in most cases, has already been studied by previous authors, and can be used as a specific heat standard. For nickel, the most precise and recently published experimental work is by Dixon *et al.*[14] reinterpreted by Bower *et al.*[15] by using new elastic constant data. Unfortunately, these authors worked only in the pumped helium temperature range (1.1–4.2 K), so no precise calibration is possible in the 4.2–10-K range on the basis of a nickel standard.

We have used Dixon's results on sample II to calibrate our apparatus, with the following equation:

$$C_V = \gamma T + \beta T^3 + \alpha T^{3/2} \tag{2}$$

where

$$\alpha = 0.029 \text{ mJ/K}^{5/2} \text{ mole} ,$$

$\beta = 0.01848$ mJ/K^4 mole ,

$\gamma = 7.024$ mJ/K^2 mole.

The preceding values have been chosen by Bower: β corresponds to the acoustic value of the Debye temperature Θ_D (472 K). The $\alpha T^{3/2}$ term is due to the ferromagnetic-spin-wave specific heat. For the sake of simplicity, no correction accounting for an energy gap due to magnetocrystalline anisotropy effects as described by Argyle *et al.*[16] has been introduced. α and γ have been optimized through a best fit of Dixon's results. The adopted value is within 10% of the computed value from neutron data (0.029 instead of 0.032).

Fortunately, sample II has approximately the same impurity content as ours, and it has the same origin (Mond Company), which makes us more confident for an identification of both samples. On the other hand, results for sample I in Dixon's paper cannot be substituted into Eq. (2) with correct values for α: The best fit gives $\alpha \simeq 0$ in this region, which cannot be correct, and probably indicates that the spin wave term is overshadowed by another effect—hyperfine interaction for instance. Unfortunately, the absence of any chemical analysis for this sample makes any physical interpretation uncertain.

Of course, this procedure is perfectly correct for the temperature range where Dixon *et al.* give their results. At higher temperatures, we cannot rely on an extrapolation of the nickel low-temperature law, first because of the inaccuracy of the method, and second because the phonon specific heat can only be represented by βT^3 for temperatures below $\Theta_D/60$. Another standard was thus required for the high temperature range, and we used the 1965 Calorimetry Conference copper standard.

One has to be careful when applying the above method to the correction of nickel experiments on the basis of a copper calibration, since $(1/C)(dC/d\Theta)$ values are obviously different. Using Eq. (1) for copper and nickel, we find $\Delta\varphi(\Theta)$, the difference between the φ functions for copper and nickel:

$$\Delta\varphi(\Theta) = \varphi_{Ni}(\Theta) - \varphi_{Cu}(\Theta)$$

$$= f(\Theta)\left[\frac{1}{C}\frac{dC}{d\Theta}\bigg|_{Ni} - \frac{1}{C}\frac{dC}{d\Theta}\bigg|_{Cu}\right].$$

$f(\Theta)$ is estimated by a numerical integration of Eq. (1). It is always less than 10^{-2} K. $\Delta\varphi$ can then be computed: Its maximum absolute value, 0.17%, is reached at about 6.5 K. Using the copper sample to calibrate the apparatus, we obtained the value for φ_{Cu} in the high-temperature region (4.2–10 K) and then deduced φ_{Ni}.

D. Accuracy

In the low-temperature region (1.2–4.2 K) we can claim an accuracy of 0.1%, while in the high-temperature range, the calibration error can

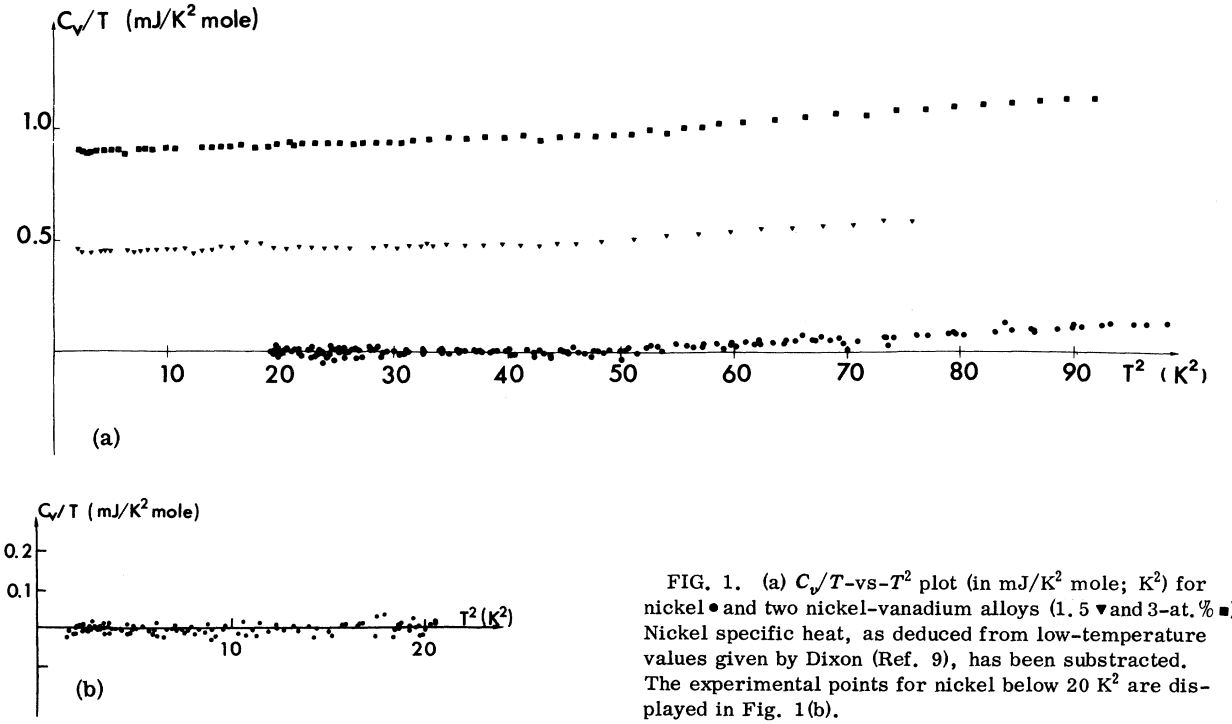

FIG. 1. (a) C_v/T-vs-T^2 plot (in mJ/K^2 mole; K^2) for nickel • and two nickel-vanadium alloys (1.5 ▼ and 3-at.% ■). Nickel specific heat, as deduced from low-temperature values given by Dixon (Ref. 9), has been substracted. The experimental points for nickel below 20 K^2 are displayed in Fig. 1(b).

amount to 0.3%, owing to the scatter of the points on the copper curve. Figure 1 gives the (C_v/T) vs T^2 plot for the experiments on pure nickel, performed over a 1-yr period, the nickel standard value given by Eq. (2) having been subtracted (the values obtained for nickel-vanadium alloys are also plotted on the same graph). The error function we used, $\varphi(\Theta)$, is the one we refer to in the preceding paragraph. The standard law is well obeyed up to 50 K^2(7 K), which corroborates our choice of nickel II (Mond) as a specific heat standard and confirms the fact that nickel I used by Dixon should be rejected.

From this plot, we deduced a *high-temperature* value for β [$(191 \pm 4) \times 10^{-4}$ mJ/K^4 mole] which is consistent, within experimental error with Bower's elastic constant measurements: $(185 \pm 3) \times 10^{-4}$ mJ/K^4 mole. It will be understood that the absolute accuracy on the *increment* of β between pure nickel and a dilute nickel alloy (1×10^{-4} mJ/K^4 mole) will be better than the absolute accuracy of β for one sample (1×10^{-4} mJ/K^4 mole) as a result of calibration errors in the 4.2–20 K range. The accuracy on γ and $\Delta\gamma$ is the same; we give them within an error of 10^{-2} mJ/K^2 mole.

IV. RESULTS

Plots similar to Fig. 1 have been drawn for all samples, and these show, except for manganese (see below), a linear dependence of C_v/T on T^2 in the temperature range where nickel obeys its standard law. This shows that the nickel spin wave term is approximately unaltered in the dilute alloys we have measured.

On these plots, the increments of the specific heat parameters $\Delta\gamma$ and $\Delta\beta$ are given respectively by the intercept with the C_v/T axis and the slope of the straight lines which represent the low-temperature limiting law of the specific heat. These results are given in Tables I(a)–I(c) for each concentration and for each transition series.

TABLE I. Increments of the low-temperature specific-heat parameters for dilute alloys for transition metals dissolved in Ni. c: impurity concentration in at.%; $\Delta\gamma$: increase of the electronic-specific-heat coefficient (in mJ/K^2 mole); $\Delta\beta$: phonon specific-heat coefficient increase (in 10^{-4} mJ/K^4 mole).

	$\Delta\gamma$ (mJ/K^2 mole)					$\Delta\beta$ (10^{-4} mJ/K^4 mole)				
				(a) First series						
c(at.%)	1	1.5	2	3	4	1	1.5	2	3	4
Ti		0.265		0.535			9		18	
V		0.445		0.895			8		16	
Cr		0.635		1.285			4		10	
Mn	−0.120		−0.215		−0.285	3		5		12
				(b) Second series						
c(at.%)	0.7	1	1.5	2	2.5	3	0.7	1	1.5	2	2.5	3
Nb	0.235		0.505		0.725		10		16		28	
Mo	0.340		0.680			1.235	8		16			30
Ru	0.200 (0.5%)	0.4					5 (0.5%)	10		22		
Rh		−0.02		−0.025				9		18		
Pd		0.025		0.055				5		9		
				(c) Third series						
c(at.%)		1		2			1			2		
Ta		0.335		0.655			13			24		
W		0.445		0.80			11.5			24		
Re		0.56 − 0.59[a]		1.025			11			19		
Os		0.68		1.33			11			19		
Ir		0.26 − 0.29[a]		0.55			− a			18		
Pt		0.13 − 0.16[a]		0.235			8			17.5		

[a]These experiments are more scattered than the others; hence a lack of precision on the corresponding parameters.

For manganese alloys, an upturn is to be noticed at low temperatures. This behavior is due to the hyperfine term, the manganese nuclei interacting with the field created at their lattice sites by the matrix magnetism. We estimated this term for each alloy using the nuclear data for manganese and the values of hyperfine fields on manganese atoms in nickel-manganese dilute alloys, measured by NMR.[17] We subtracted from the specific-heat data the quantity[18]

$$C_H = \tfrac{1}{3} N k_B \frac{I+1}{I}\left(\frac{\mu_B}{k_B T}\right)^2 \langle H^2 \rangle ,$$

$\langle H^2 \rangle$ being the mean-square value of the magnetic field at the manganese nuclei. This accounts for field variations from site to site, owing to Mn-Mn interactions. With this correction, the 1-at.% curve was fairly linear, but the 2 and 4-at.% curves retained slight upturns. The deviations could be analyzed as being proportional to the square of the concentration, reaching $C_H T^2 = 0.1$ mJ K for the 4-at.% sample. The effect is much too strong to be explained by quadrupolar interactions with gradients due to lattice distortions induced by manganese neighbors. We must conclude that the origin of the effect is magnetic, the mean-square hyperfine field being stronger than the value calculated from Streever's paper. Supposing that the extra effect is due to manganese nuclei with one manganese neighbor, our experiments yield a hyperfine field of 440 kG at these nuclei. The corresponding frequency is high and the resonance could have been missed by Streever. This is not unlikely, since the analysis he gave for the concentration dependence of the line intensities is not altogether convincing, and the relative increases he gave for the mean frequency at 4.2 K are approximately ten times smaller than the saturation moment relative increases. Anyway, the manganese alloy specific heat parameters displayed in Table I(a) are calculated from corrected curves, using values of the nuclear specific heat which ensure the linearity of the C_V/T vs T^2 plots.

The result which is of fundamental interest for the study of dilute alloys is given by the slope at infinite dilution $d\gamma/dc\,|_0$ of the γ-vs-concentration curves. These curves are plotted in Figs. 2(a)–2(c) for the three transition-series elements, and the corresponding slopes are plotted in Figs. (3a)–(3c). For comparison purposes, the latter figures also show Durand's results[19] for $\rho_{0\downarrow}$, the residual resistivity in the ($\downarrow$) band per unit concentration of the considered impurity.

V. DISCUSSION

A. Period Effect

In the Introduction we have seen, on the basis of magnetization results, that the virtual bound state crosses the Fermi level for chromium in the first series, for ruthenium in the second, and for osmium in the third. Specific-heat results are in good agreement with this picture for the first and third series. For the second, both specific-heat and resistivity results suggest that the increase of the density of states at the Fermi level might be

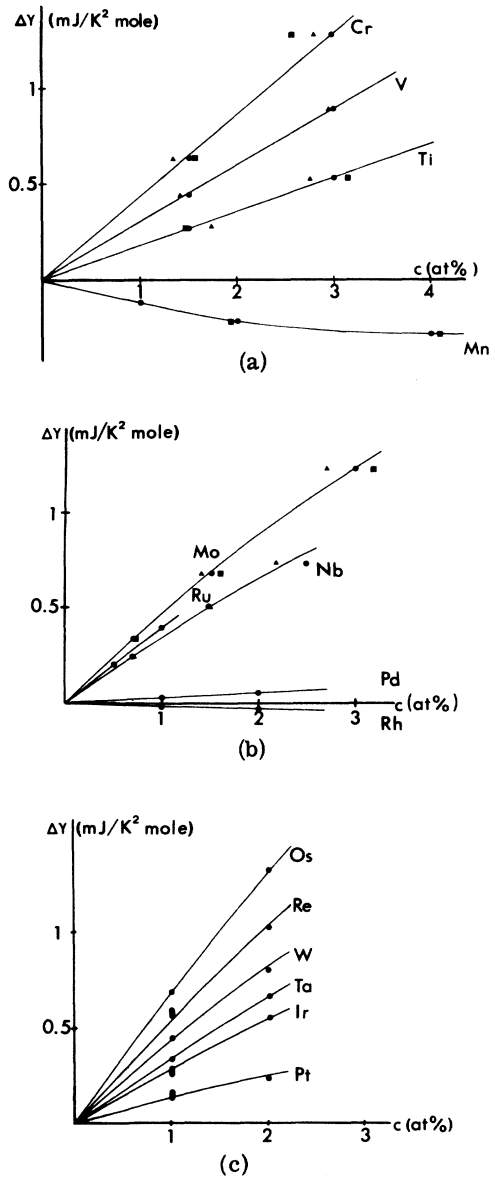

FIG. 2. Electronic specific-heat coefficient increment $\Delta\gamma$ (mJ/K^2 mole) vs concentration for dilute alloys of transition metals dissolved in nickel. (a) First series—symbols: •, nominal concentration; ■, chemical analysis; ▲, spectrometric analysis. (b) Second series: same symbols. The value of the concentration for the 2.5-at.%-Nb alloy is doubtful. (c) Third series—nominal concentrations.

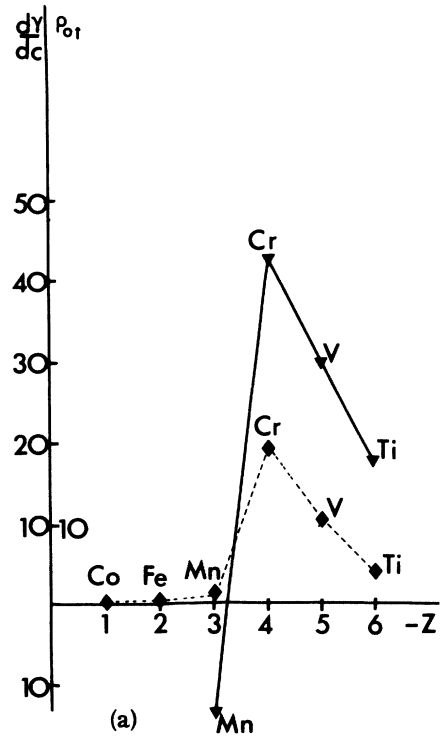

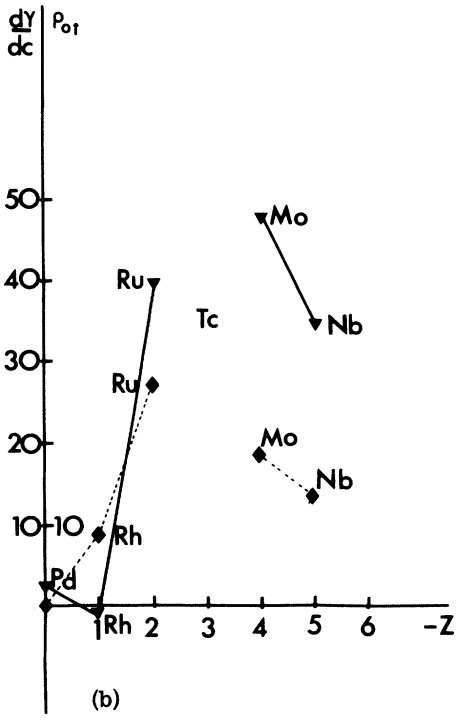

even larger for technetium than for ruthenium. This is, however, at variance with Cadeville's thermoelectric-power results, which give $S_{0t} \simeq 0$ for ruthenium.

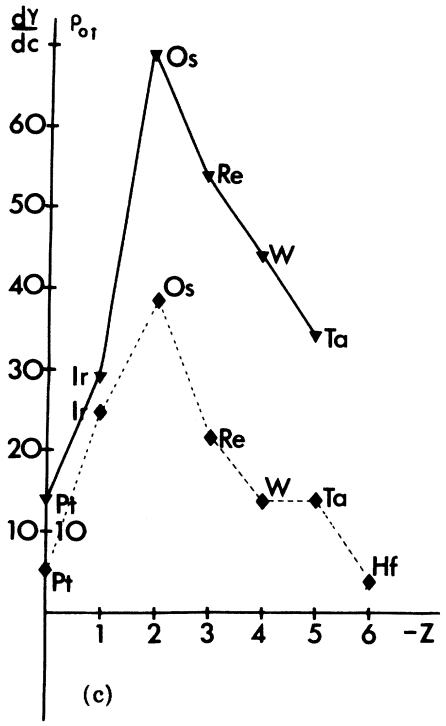

FIG. 3. Values of ρ_{0t}, specific residual resistivity relative to the transitional impurities in Nickel for the (t) band (in $\mu\Omega$cm per at.% impurity) ♦ and low-concentration values of $d\gamma/dc\,|_0$ specific increment of electronic specific heat (in mJ/K^2 mole per unit atomic concentration) ▼. (a): first series; (b): second series; (c): third series.

B. Interaction Effects between Impurities

A nonlinear dependence of γ with c is due to interactions between impurities. If we trust the nominal concentrations of the samples, Fig. 2 clearly indicates that such effects are absent for all of the first-series alloys, except manganese. For this element the interaction effects are so important that earlier studies by Beck[20] at rather high concentration gave a positive value of $d\gamma/dc\,|_0$, whereas ours is negative. This curvature could be related to the peculiar behavior of manganese atoms, Mn-Ni interactions being ferromagnetic and Mn-Mn antiferromagnetic. Some reservations should, however, be kept on this point since manganese residual resistivity in nickel is linear up to 5%.

For the second and third series, pair effects do show up for all alloys, at least when large values of $d\gamma/dc$ allow for a reasonable resolution of second-order effects. This behavior is different from that of the first-series alloys and can be explained by the fact that the radial extension of the

atomic orbitals is larger for the second and third series than for the first. This effect remains true in the nickel matrix, and the perturbations created around the impurities would interact more easily for the second and third series. It is worth mentioning that deviations to linearity for the impurity resistivity, with the exception of the case of ruthenium, do not show up until 5%, which is somewhat different from what we observe in our experiments.

C. Study of $d\gamma/dc|_0$ Values

Here we must remember that both (↑) and (↓) bands may contribute to the $d\gamma/dc|_0$ values. We can write $d\gamma/dc|_0 = \gamma_{0\uparrow} + \gamma_{0\downarrow}$.

1. Alloys with Virtual Bound State Sitting at Fermi Level

In this case, as the virtual bound state induces a strong γ increase, we can identify $d\gamma/dc|_0$ and $\gamma_{0\uparrow}$ without introducing too important an error. If we assume that the virtual bound state has a Lorentzian shape and is normalized to five states, it is possible to give an estimate of its width from the height of the $\gamma_{0\uparrow}$ peak. For chromium, assuming the virtual bound state to be centered on the Fermi level, we find a maximum width of $\Delta = 0.14$ eV, using our 43 mJ/K^2 mole per unit concentration value. This result fits in with Cadeville's estimate from thermoelectric-power measurements.[5] This is very surprising since the values for virtual-bound-states widths are expected to be found between 0.5 and 1 eV. The discrepancy is even greater if we consider that, for chromium, only one out of the five states of the virtual bound level is filled (as shown both by saturation moments and by the high thermoelectric power measured by Cadeville), so that the $\gamma_{0\uparrow}$ value to be used should be still higher and the width smaller. On the other hand, Demangeat[21] has made a calculation from first principles on nickel-chromium alloys. He found a non-Lorentzian density for the virtual bound state, with the Fermi level on the rising part of the curve (in agreement with Cadeville's thermopower measurements). Owing to the assymmetrical nature of the curve, the density of states at the Fermi level does not differ very much from its maximum value, but there is still a discrepancy by a factor of 8 with our experimental values.

The results for ruthenium alloys are nearly the same as for chromium alloys, and the width we can deduce is then similar. The comparison with theory leads to similar discrepancies; things would be even worse in the second than in the first series, due to the fact that the virtual bound states should be broader, the impurity orbitals showing larger spatial extension and inducing an energy broadening through an increase of V_{sd} [$\Delta = |V_{sd}|^2 \times n_s(E_F)$].[22] We cannot compare the *width* we find with thermopower results since the virtual bound state is half-filled ($Z_\uparrow = -2.5$) and the thermopower then close to zero.

For the third series, unlike the first, the virtual bound state remains at the Fermi level for two elements: osmium ($Z_\uparrow = -2$) and rhenium ($Z_\uparrow = -4.5$). This indicates, as expected, that this state is broader again for the third series. This is corroborated by thermopower results, the estimated widths in the Lorentzian approximation being 0.3 eV for osmium and 0.5 eV for rhenium, more than twice the value for chromium. It is again smaller than the expected value of 1 eV. Our results do not agree with these estimates, as we find 69 mJ/K^2 mole per unit impurity for osmium and 54 mJ/K^2 mole for rhenium, these values being even larger than for chromium.

We can on the whole conclude that, when the virtual bound state sits on the Fermi level, our measurements yield density-of-states values higher than expected, leading to smaller level widths. This indication is consistent with other types of experiments: The same contradiction shows up for dilute solutions of transition metals in nontransition matrices. An exhaustive study on aluminium-base alloys by Aoki *et al.*[23] (specific heat, resistivity, magnetic susceptibility, and superconducting temperature) leads to $\Delta = 0.2$ eV. On gold-nickel, Caroli[24] found $\Delta = 0.14$ eV by resistivity and near-infrared absorption methods.

2. Alloys with Empty Virtual Bound State

This situation prevails when $|Z| \leq 5$ (vanadium) in the first series and $|Z| \leq 4$ (molybdenum, tungsten) in the two others. In this range, the virtual bound state being far from the Fermi level, we should not expect any effect on γ. This is not the case, however, as our curves show that, although smaller than the "VBS on" values, the $d\gamma/dc|_0$ values are still quite large. One could argue that for titanium, as $Z_\downarrow = -1$, the increase is due to (↓) band effects, but if we compute an estimate of $\gamma_{0\downarrow}$ as in Sec. IV C 3, we find -7.3 mJ/K$^2 \times$mole (as for cobalt). We could reach another estimate of this (↓) band effect through the study of nickel-copper alloys,[25] but the order of magnitude of this estimate is too small to give any satisfactory explanation. It is interesting to note that the $\rho_{0\downarrow}$ values are also rather important. This indicates, as in the preceding paragraph, that non-*d* effects show up.

Similar problems arise for the neutron-diffraction experiments. We know that, in a pure-*d* model, the closer the impurity level to the top of the band, the broader should be the spatial extension of the magnetic perturbation induced by the im-

purity. In fact, neutron diffraction does not show any variation of the spatial distribution of the magnetic moment. Again, the experiment cannot be interpreted within the frame of pure-d effects.

3. *Alloys without Virtual Bound State Effects*

For manganese we find a $d\gamma/dc\,|_0$ value of -13 mJ/K^2 mole per unit concentration. It should be interesting to correlate this value with existing results for other alloys and with the state of the theory. This was attempted by Gomes and Campbell,[26] who found a good agreement with their model for iron and cobalt impurities in nickel, but failed to explain the positive result for manganese found by Beck at high concentration. As the result is in fact negative, it can then be explained in the following way. Since we have

$$\left.\frac{d\gamma}{dc}\right|_0 = \left(A + B\tan\frac{\pi Z_\downarrow}{5}\right)\sin\frac{2\pi Z_\downarrow}{5} \quad ,$$

as deduced from formula (18) in Gomes's paper, where A and B are parameters which depend only on the nickel band structure, and $Z_\downarrow$ is taken as equal to Z ($Z_\uparrow$ being neglected). With two experimental values of $d\gamma/dc\,|_0$, it is possible to calculate A and B and to deduce the $d\gamma/dc\,|_0$ value for any other impurity.

For cobalt-nickel alloys ($Z=-1$), $d\gamma/dc\,|_0 = -7.3$ mJ/mole K^2.[11] For iron-nickel alloys ($Z=-2$), $d\gamma/dc\,|_0 = -15$, as given by Ref. 15. We can thus deduce a value for nickel-manganese alloys (-12.5) which is very close to the experimental value (-13). This gives surprisingly good agreement, since the model accounts only for the screening in the impurity cell, but fails when applied to second- and third-series impurities. Besides, the fit between our values for A and B and the band-structure parameters as computed by Demangeat[27] for nickel is rather poor.

D. Phonon Parameters

It has been noticed that when an impurity is replaced by a heavier isoelectronic one, the phonon term increases, this being a trivial mass effect. Less trivial is the phonon-term increase within a transition series, when an impurity is replaced by a lighter one. This effect, which means that lighter impurity atoms are responsible for softer modes, is not clearly understood. It could be explained by assuming that local cohesion is reduced by emptying ($\downarrow$) levels, allowing for softer local vibration modes on the impurity.

Alternatively, we remember that, when the impurity becomes lighter (within a series), its atomic radius increases. This difference in size induces relaxation effects in the solvent lattice and the frequencies of some nickel atom modes could be lowered. In the first model, Θ_D should remain approximately constant until $|Z|$ reaches the critical value, then decrease rather steeply. In the second one, Θ_D should vary continuously. The accuracy of our measurements does not allow us to distinguish between the two explanations.

VI. CONCLUSIONS

The agreement between our specific-heat experiments and the present state of the theory of transition-metal dilute alloys in nickel is only qualitative. A hump of the electronic specific-heat curve is clearly related to the crossing of the Fermi level by the virtual bound state, but the order of magnitude of the effect is systematically too large. This indicates both a virtual level narrower than predicted theoretically and the presence of other effects increasing the γ coefficient.

A similar contradiction between theory and practice exists for dilute nontransition base alloys.

ACKNOWLEDGMENTS

The authors wish to thank Professor J. J. Veyssié for his advice about the design of the equipment, and Professor F. Gautier for extensive discussions on the results of our experiments.

*Work written in partial fulfillment of the Doctorat-es-Sciences Physiques of R. Caudron, Université Louis Pasteur, Strasbourg.

[1] J. Friedel, *Proc. of the Int. School of Physics, Varenna, Italy, 1967 "Enrico Fermi,"* Course 37 (Academic, New York, 1967), p. 283.

[2] P. W. Anderson, Phys. Rev. **124**, 41 (1961).

[3] C. Demangeat and F. Gautier, J. Phys. (Paris) **31**, 903 (1970).

[4] J. Crangle and D. Parsons, Proc. R. Soc. Lond. **255**, 509 (1960).

[5] M. C. Cadeville, F. Gautier, C. Robert, and J. Roussel, Solid State Commun. **7**, 1701 (1969).

[6] A. Fert and I. A. Campbell, Phys. Rev. Lett. **21**, 1190 (1968).

[7] J. Durand and F. Gautier, J. Phys. Chem. Solids **31**, 277 (1970).

[8] M. Hansen, *Constitution of Binary Alloys* (McGraw-Hill, New York, 1958).

[9] M. Dixon, F. E. Hoare, and T. M. Holden, Proc. R. Soc. A **303**, 339 (1968).

[10] J. C. Ho and R. Viswanathan, Phys. Rev. **172**, 705 (1968).

[11] R. Caudron, J. J. Meunier, and P. Costa (unpublished).

[12] R. Caudron, F. Ducastelle, and P. Costa, J. Phys. Chem. Solids **31**, 291 (1970).

[13] J. C. Holste, J. C. Cetas, and C. A. Swenson, Rev. Sci. Instr. **43**, 670 (1972).

[14] M. Dixon, F. E. Hoare, T. M. Holden, and D. E. Moody, Proc. R. Soc. A **285**, 561 (1965).

[15] D. J. Bower, E. Claridge, and I. S. T. Tsang, Phys. Status Solidi **29**, 617 (1968).

[16] B. E. Argyle, S. H. Charap, and E. W. Pugh, Phys. Rev. **132**, 2051 (1963).

[17] R. L. Streever, Phys. Rev. **173**, 591 (1968).

[18] O. V. Lounasmaa, in *Hyperfine Interactions*, edited by A. Freeman and R. Frenkel (Academic, New York, 1967), p. 467.

[19] J. Durand, Thèse (University of Strasbourg, 1969) (unpublished).

[20]K. P. Gupta, C. H. Cheng, and P. A. Beck, J. Phys. Chem. Solids **25**, 73 (1964).
[21]C. Demangeat, First European Conference on the Physics of Condensed Matter, Florence, 1971 (unpublished).
[22]V_{sd} is the matrix element of the perturbating potential between the s states of the matrix and the d states of the impurity.
[23]R. Aoki and J. Ohtsuka, J. Phys. Soc. Jap. **26**, 651 (1969).
[24]B. Caroli, Ref. 169 of G. J. Van den Berg, in *Progress in Low Temperature Physics*, edited by C. Gorter (North-Holland, Amsterdam, 1964).
[25]K. P. Gupta, C. H. Cheng, and P. A. Beck, Phys. Rev. **133**, A203 (1963).
[26]A. A. Gomes and I. A. Campbell, J. Phys. C **1**, 253 (1968).
[27]C. Demangeat (private communication).